Orientational multiplicity and transitions in liquid crystalline droplets

Rajesh K. Goyal and Morton M. Denn
Benjamin Levich Institute for Physico-Chemical Hydrodynamics and Department of Chemical Engineering, City College of New York, CUNY, New York, New York 10031, USA
(Received 18 October 2006; published 28 February 2007)

Orientation distributions in droplets of liquid crystals with homeotropic anchoring are computed with a simulated annealing algorithm that minimizes the free energy of the Oseen-Frank continuum theory. The droplets exhibit multiple orientational steady states that are separated by finite energy barriers over the entire range of the dimensionless ratio of surface to elastic forces, with maximum transition energy densities of the order of 2000 J/m^3 (Pa) for a typical liquid crystalline droplet with a spherical radius of 1 μm. The transition energy densities decrease with elongation to spheroidal droplets with aspect ratios of four or more, indicating that droplet elongation is favored to drive surface-induced transitions.

DOI: 10.1103/PhysRevE.75.021704 PACS number(s): 61.30.Gd, 61.30.Pq

I. INTRODUCTION

A. Nematic droplets

Droplets of a nematic liquid crystal dispersed in an isotropic matrix are of interest in a variety of technologies and control of the liquid crystal orientation in the droplet is an essential feature for applications. The orientation is determined by a balance between the bulk nematic potential, which favors alignment, and the surface potential, which often favors an orthogonal (*homeotropic*) orientation. The orientational issues in liquid crystalline droplets are discussed in a brief review by Lavrentovich [1] and in more detail in the book by Drzaic [2].

Multiple locally stable states can exist in liquid crystalline droplets. We have recently found bistability in a dispersion of the biphenylcarbonitrile 8CB in polydimethylsiloxane [3], for example, where dispersed droplets with a radial conformation or a bicontinuous gel-like morphology can both exist. We explore here the orientational morphologies of spherical and spheroidal droplets of low molar-mass liquid crystals using a simulated annealing approach, with particular attention paid to bistability and the transitions between locally stable states.

B. Free energy

Nematic order in a low molar mass liquid crystal is described by a position-dependent unit vector **n**, known as the *director*. The free energy density of a bulk nematic can be expressed in terms of **n** by the Oseen-Frank continuum theory [4],

$$f = \frac{1}{2}[k_{11}(\nabla \cdot \mathbf{n})^2 + k_{22}(\mathbf{n} \cdot \nabla \times \mathbf{n})^2 + k_{33}(\mathbf{n} \times \nabla \times \mathbf{n})^2 - k_{24}\nabla \cdot (\mathbf{n} \times \nabla \times \mathbf{n} + \mathbf{n}(\nabla \cdot \mathbf{n}))], \quad (1)$$

where the Frank elastic constants k_{11}, k_{22}, k_{33}, and k_{24} are associated with splay, twist, bend, and saddle-splay distortions, respectively. [Our k_{24} is twice the saddle-splay coefficient defined by Kleman and Lavrentovich [4]. A mixed-splay-bend term with an elastic coefficient k_{13} is usually neglected because it involves higher-order derivatives of the director field. The apparent higher-order saddle-splay terms in Eq. (1) reduce in fact to first derivatives of the vector field.] **n** and **−n** must be equivalent in a nematic.

When all four elastic constants are equal to a single constant K, the bulk free energy density simplifies to

$$f = \frac{1}{2}K(\nabla \mathbf{n}):(\nabla \mathbf{n})^T. \quad (2)$$

The assumption of equal constants is only approximate for real liquid crystals; for 4′-pentyl-4-biphenylcarbonitrile (5CB), for example, values of $k_{33}/k_{11}=1.6$ and $k_{22}/k_{11}=0.48$ [4], $k_{33}/k_{11}=1.31$ and $k_{22}/k_{11}=0.51$ [5], and $k_{33}/k_{11}=1.4$ and $k_{22}/k_{11}=0.66$ [6] have been reported. The ratio k_{33}/k_{11} appears to be of order 0.1, and k_{22}/k_{11} less than 10^{-2}, in a liquid crystalline copolyesteramide [7].

The saddle-splay constant k_{24} has received less attention than the other elastic coefficients, in part because the saddle-splay term can be expressed as a divergence that integrates to a surface integral and is thus often neglected, but the term can be important in nonplanar geometries. Saddle-splay effects are reviewed broadly in Crawford and Žumer [8]. Data for k_{24} are quite limited; Polak and co-workers [6] estimate $k_{24}/k_{11} \sim 3.1$ for 5CB using an optical method, but note that various bounding estimates would result in $1.2 > k_{24}/k_{11} > 0.9$. [They expressed their bounds in terms of $2k_{24}/(k_{11}+k_{22})$, and we have used the reported values of k_{22}/k_{11} for 5CB to rewrite the inequalities as shown here. The upper bound is derived from an inequality by Ericksen [9] that requires that k_{24} be less than twice the smaller of k_{11} or k_{22}. The Ericksen inequality is violated by the result obtained from their optical measurements.] The Cauchy relation $k_{24} = \frac{1}{2}(k_{11}+k_{22})$ [10] is often assumed, and this relation is roughly consistent with ^{2}H-NMR measurements summarized by Crawford and Žumer [8] for a deuterated 5CB.

The surface free energy density of a nematic at an interface with a preferred radial orientation is usually given by the single-constant Rapini and Papoular [11] form,

$$f_S = \frac{1}{2}W \sin^2 \varphi, \quad (3)$$

where W is a constant and φ is the angle between the director $\mathbf{n}$ and the preferred interfacial orientation (the *easy direction*); this is a convenient functional form for the surface free energy, in that it is bounded and approximates a leading-order quadratic term for small angles. $\mathbf{n}$ minimizes the total free energy, which is the sum of the volume integral of f and the surface integral of f_S.

C. Transitions

The equilibrium nematic orientation in a droplet is determined by the relative strengths of the surface and bulk forces. It is helpful to consider two orientation distributions for which the free energy can be calculated analytically in a spherical droplet of radius R with radial anchoring. One is a radial (or *hedgehog*) orientation, with a singularity at the center; here the bulk contribution to the free energy equals $4\pi R(2k_{11}-k_{24})$ and the surface free energy is zero, so the total free energy is $4\pi R(2k_{11}-k_{24})$. The other is a perfectly parallel orientation, for which the bulk free energy is zero and the surface (and total) free energy is $4\pi WR^2/3$. According to these values, the radial orientation is energetically favored if $WR/(2k_{11}-k_{24})>3$ and the parallel orientation is favored if $WR/(2k_{11}-k_{24})<3$. Hence we expect an orientational transition when $WR/(2k_{11}-k_{24})$ is equal to 3. [A perfectly radial orientation is possible in principle, but there must be some deviation from a perfectly parallel orientation in the neighborhood of the surface, reducing the surface free energy and introducing a small bulk free energy contribution. Hence the actual transition is expected to occur at a value of $WR/(2k_{11}-k_{24})$ that is greater than 3.] Heppenstall-Butler *et al.* [12] and Tixier *et al.* [13] attribute different coalescence properties of small and large nematic droplets to such a structural transition.

II. COMPUTATIONAL ALGORITHM

A. Discretization

We have employed a simulated annealing approach to finding the minimizing vector field $\mathbf{n}$ in a liquid crystal droplet by discretizing the free energy and seeking the minimum with a Metropolis Monte Carlo algorithm. The droplet is circumscribed by a rectangular parallelepiped that is discretized into cubes of equal volume, and the vector field $\mathbf{n}$ is defined by a discrete value in each element. The centroid of the droplet is located at the intersection of eight central elements (four faces in each coordinate plane), and a cubic element is considered to be contained within the droplet if the centroid of the element lies within the droplet. The curved surface of the droplet can be closely approximated by this method with sufficiently fine discretization. Only directors in the outermost layer of elements experience the surface potential [Eq. (3)]. [The discretized macroscopic free energy is formally similar to the Lebwohl-Lasher (LL) molecular model for liquid crystals [14–16], in which molecules on a cubic lattice interact through a nearest pair potential, but the molecular model is not appropriate for macroscopic droplet calculations. The LL model admits a nematic-isotropic phase transition ([17] and references therein).]

Straightforward discretization of the free energy density in Eqs. (1) and (2) results in loss of equivalence of $\mathbf{n}$ and $-\mathbf{n}$. Hobdell and Windle [18] proposed rotating one of the vectors through 180° whenever two vectors are at a relative angle of more than 90°. We follow instead a procedure by Gruhn and Hess [19] to retain nematic symmetry. (Hobdell and Windle and Gruhn and Hess did not include the k_{24} term.) Equation (1) can be rewritten as

$$f=\frac{1}{2}[k_{22}(\nabla\mathbf{n}):(\nabla\mathbf{n})^T+(k_{33}-k_{22})(\mathbf{n}\times\nabla\times\mathbf{n})^2+(k_{11}-k_{22})(\nabla\cdot\mathbf{n})^2+(k_{24}-k_{22})((\nabla\mathbf{n}):(\nabla\mathbf{n})^T-(\nabla\cdot\mathbf{n})^2-(\nabla\times\mathbf{n})^2)], \quad (4)$$

which, because of the unit magnitude of $\mathbf{n}$, is equivalent to

$$f=\frac{1}{2}\left[\frac{1}{2}k_{22}(\nabla_\alpha n_\beta n_\gamma)(\nabla_\alpha n_\beta n_\gamma)+\frac{1}{2}(k_{33}-k_{11})(n_\alpha n_\beta)(\nabla_\alpha n_\gamma n_\nu)(\nabla_\beta n_\gamma n_\nu)+(k_{11}-k_{22})(\nabla_\alpha n_\alpha n_\gamma)(\nabla_\beta n_\beta n_\gamma)\right.$$
$$\left.+(k_{24}-k_{22})((\nabla_\alpha n_\beta n_\gamma)(\nabla_\beta n_\alpha n_\gamma)-(\nabla_\alpha n_\alpha n_\gamma)(\nabla_\beta n_\beta n_\gamma))\right]. \quad (5)$$

We have used subscript notation and the Einstein summation convention to avoid ambiguity. Equation (5) retains the equivalence of $\mathbf{n}$ and $-\mathbf{n}$ following discretization.

Gruhn and Hess proposed implementing both forward and backward differences to approximate derivatives and averaging over eight terms involving nearest neighbors. We find that it is adequate to average over two nearest neighbor terms, as follows: The discretized bulk energy density at each lattice point is

$$f(i,j,k)=\frac{1}{4l^2}\sum_{(r,s,t)\varepsilon[(1,1,1),(-1,-1,-1)]}\left\{\frac{1}{2}k_{22}\sum_{\beta,\gamma=1}^{3}\sum_{\alpha=1}^{3}\left(A^{(r,s,t)}_{(\alpha\beta\gamma)}(i,j,k)\right)^2+(k_{11}-k_{24})\sum_{\beta=1}^{3}\left(\sum_{\alpha=1}^{3}A^{(r,s,t)}_{(\alpha\alpha\beta)}(i,j,k)\right)^2\right.$$
$$\left.+\frac{1}{2}(k_{33}-k_{11})\sum_{\beta,\gamma=1}^{3}\left(\sum_{\alpha=1}^{3}n^{(r,s,t)}_{\alpha}(i,j,k)A^{(r,s,t)}_{(\alpha\beta\gamma)}(i,j,k)\right)^2+(k_{24}-k_{22})\left(\sum_{\alpha=1}^{3}\sum_{\beta=1}^{3}\sum_{\gamma=1}^{3}A^{(r,s,t)}_{(\alpha\beta\gamma)}A^{(r,s,t)}_{(\beta\alpha\gamma)}\right)\right\}. \quad (6)$$

TABLE I. Coefficients of free energy terms of a hedgehog point defect [Eq. (10a)] computed using 2×10^5 lattice cells.

	Analytical	Simulation (Gruhn and Hess's algorithm)	Simulation (this algorithm)
Splay ($\pi k_{11}R$)	8.0000	7.8785	7.8780
Twist ($\pi k_{22}R$)	0.0000	0.0326	0.0323
Bend ($\pi k_{33}R$)	0.0000	0.0204	0.0201
Saddle-splay ($\pi k_{24}R$)	−4.0000	−3.9833	−3.9833
Total	4.0000	3.9482	3.9471

Here l is the lattice spacing and the symbols $A^{(r,s,t)}_{(i\beta\gamma)}$ are defined as

$$A^{(r,s,t)}_{(1\beta\gamma)}(0,0,0) = n_\beta n_\gamma(r,0,0) - n_\beta n_\gamma(0,0,0),$$

$$A^{(r,s,t)}_{(2\beta\gamma)}(0,0,0) = n_\beta n_\gamma(0,s,0) - n_\beta n_\gamma(0,0,0),$$

$$A^{(r,s,t)}_{(3\beta\gamma)}(0,0,0) = n_\beta n_\gamma(0,0,t) - n_\beta n_\gamma(0,0,0). \quad (7)$$

The total free energy of the system is then approximated by

$$E = \sum_{\text{All lattices}} f(i,j,k)l^3 + \frac{1}{2}\sum_{\text{Surface lattices}} Wl^2 \sin^2\varphi. \quad (8)$$

In the single constant approximation, $k_{11}=k_{22}=k_{33}=k_{24}=K$, the total free energy of the system is approximated by

$$E = \frac{Kl}{4}\sum_{\text{All lattices}}\sum_{\text{Six NN of (i,j,k)}}[1-(\mathbf{n}(i,j,k)\cdot\mathbf{n}(l,m,n))^2] + \frac{1}{2}\sum_{\text{Surface lattices}} Wl^2\sin^2\varphi, \quad (9)$$

where (l,m,n) is the nearest neighbor (NN) of (i,j,k).

B. Accuracy

We have tested the accuracy of the discretization by entering the analytical director distributions for two defect structures, the hedgehog (radial) and col (hyperbolic), respectively, using the discretization to calculate the relative contributions to the bulk free energy densities, which are as follows:

Hedgehog: $\mathbf{n} = (x,y,z)/(x^2+y^2+z^2)^{1/2}$,

$$E_b = 4\pi R(2k_{11}-k_{24}), \quad (10a)$$

Col: $\mathbf{n} = (-x,y,z)/(x^2+y^2+z^2)^{1/2}$,

$$E_b = 8\pi R\left(\frac{k_{11}}{5}+\frac{2k_{33}}{15}+\frac{k_{24}}{6}\right). \quad (10b)$$

A comparison of the analytical values for the coefficients of the various terms in the free energy densities with computed values using 2×10^5 lattice cells is shown in Tables I and II. The computed values using Gruhn and Hess's algorithm are also shown. The computed results are in good agreement with the analytical values, and the two algorithms have comparable accuracy. (We assume throughout this study that the center singularity, which is permitted by the Frank formalism, is attainable. In a physical system there is likely to be a small defect core.)

C. Free energy minimization

The system is initialized by choosing the vectors $\mathbf{n}(i,j,k)$ randomly, or by choosing a specific distribution (a parallel or radial orientation, for example). We then randomly choose a lattice cell and randomly change the orientation of the director within that cell. This move affects the free energy density in the selected cell and the six nearest neighbors. The new director orientation is accepted or rejected according to Metropolis sampling, in which the new orientation is accepted with probability $p(\mathbf{n}_{\text{old}}\rightarrow\mathbf{n}_{\text{new}})=\min[1,\exp-(\Delta E/k_BT)]$. Temperature enters the mean-field Oseen-Frank theory only implicitly through the temperature dependence of the physi-

TABLE II. Coefficients of free energy terms of a col point defect [Eq. (10b)] computed using 2×10^5 lattice cells.

	Analytical	Simulation (Gruhn and Hess's algorithm)	Simulation (this algorithm)
Splay ($\pi k_{11}R$)	1.6000	1.5716	1.5714
Twist ($\pi k_{22}R$)	0.0000	−0.0078	−0.0090
Bend ($\pi k_{33}R$)	1.0667	1.0580	1.0575
Saddle-splay ($\pi k_{24}R$)	1.3333	1.3277	1.3277
Total	4.0000	3.9495	3.9476

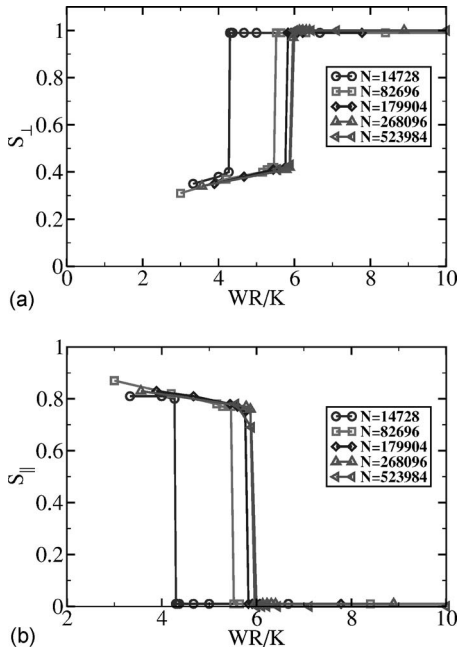

FIG. 1. (a) Radial order parameter $S_\perp$ and (b) global order parameter $S_\parallel$ as functions of the anchoring strength parameter WR/K for various discretizations.

cal constants, and fluctuations are not accounted for; hence T is a fictitious temperature (*the Monte Carlo temperature*) that is dependent on the lattice spacing. We initially fix the Monte Carlo temperature at a high value to keep the system from becoming trapped in a local minimum, and the temperature is then gradually decreased.

The algorithm becomes inefficient as the system approaches the global free energy minimum, since increasing numbers of trial moves are rejected; in that case, a scale factor is introduced to restrict the magnitude of the change in the orientation of **n**. The scale factor is adjusted to permit acceptance of about 50 percent of the trial moves during the simulations. The evolution of the total free energy and other observables are obtained by computing averages over a specified number of MC cycles, typically 20 000.

The calculations are carried out in dimensionless form. It is straightforward to show for the case of a spherical droplet of radius R with equal elastic coefficients that the only parameters (other than the dimensionless Monte Carlo temperature) are the lattice spacing l and the dimensionless group WR/K. Hence changing the drop radius with a fixed lattice spacing and changing the number of lattice sites for a fixed drop size are equivalent calculations.

D. Order parameters

Nematic order is conventionally described by a global order parameter $S_\parallel$ (usually denoted S), which equals unity when all directors are parallel and zero when the directors are oriented randomly. We use the Zannoni approach [20] to calculate $S_\parallel$. We first calculate the average order matrix $S_{\alpha\beta}$ over the N lattice points, as follows:

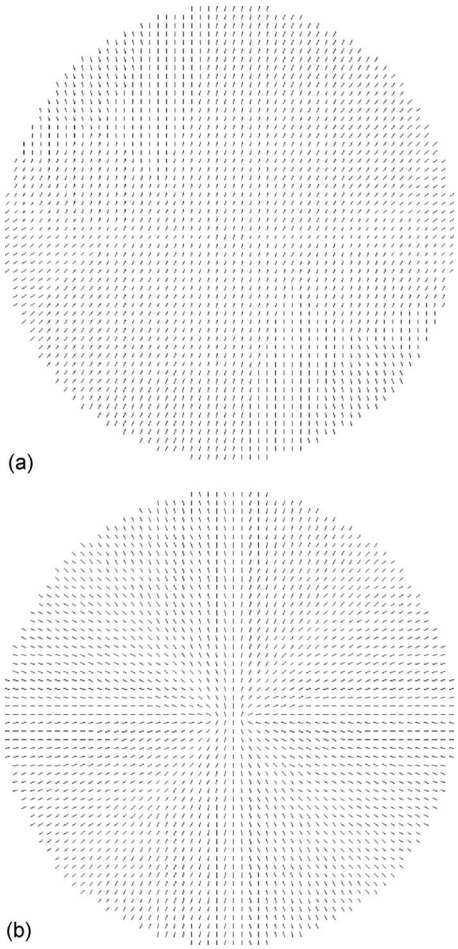

FIG. 2. Director orientation for homeotropic anchoring with (a) $WR/K=4.2$ and (b) $WR/K=6.0$.

$$S_{\alpha\beta} = \frac{1}{N}\sum_{i=1}^{N} n_{\alpha i} n_{\beta i} - \frac{1}{3}\delta_{\alpha\beta}. \tag{11}$$

Here $n_{\alpha i}$ is the projection of the unit vector on the coordinate axes, where $\alpha, \beta = x, y, z$, and $\delta_{\alpha\beta}$ is Kronecker's delta. $S_{\alpha\beta}$ is a symmetric matrix with zero trace. The global order parameter $S_\parallel$ is then defined in terms of the largest eigenvalue λ_1 of $S_{\alpha\beta}$ by

$$S_\parallel = \frac{3}{2}\lambda_1. \tag{12}$$

$S_\parallel$ equals zero not only for a random orientation, but also when the orientation is radial. Chiccoli and co-workers [21] introduced an orthogonal order parameter, which we denote $S_\perp$, defined for ellipsoids as follows:

$$S_\perp = \frac{1}{N}\left\langle \sum_{i=1}^{N} \left[\frac{3}{2}(\mathbf{n}_i \cdot \mathbf{r}_i)^2 - \frac{1}{2} \right] \right\rangle. \tag{13}$$

Here $\mathbf{r}_i$ is the local normal to the concentric ellipsoid passing through the center of the ith lattice cell. In the case of a sphere, $\mathbf{r}_i$ will always be a radial vector. Thus, for a radial orientation in a spherical geometry, $S_\perp$ is unity and $S_\parallel$ is zero; for a uniform orientation, $S_\parallel$ is unity and $S_\perp$ is zero. It is

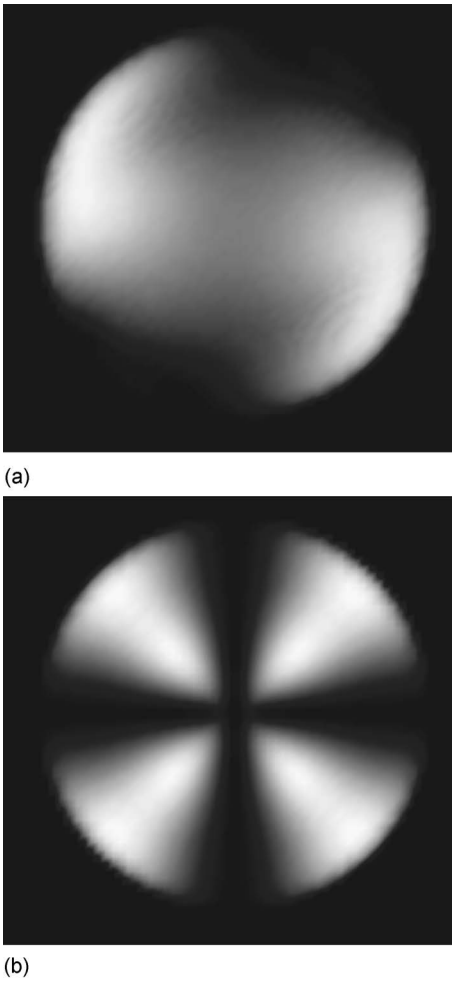

FIG. 3. Simulated polarized optical micrographs for homeotropic anchoring with (a) $WR/K=4.2$ and (b) $WR/K=6.0$.

possible for $S_{\|}$ and $S_{\perp}$ to have comparable values in an ellipsoidal geometry with a large aspect ratio.

III. RESULTS FOR SPHERICAL DROPLETS

A. Spherical droplets with orthogonal (*homeotropic*) surface anchoring

The calculated order parameters $S_{\|}$ and $S_{\perp}$ are shown as functions of WR/K in Figs. 1(a) and 1(b), respectively, for a spherical droplet with orthogonal surface anchoring and equal elastic coefficients. Random initial conditions were used for these calculations, which were carried out with 14 328, 82 696, 179 904, 268 096, and 523 984 lattice cells, corresponding to 2792, 8872, 14 936, 19 328, and 31 216 surface cells, respectively. There is convergence with respect to the number of lattice sites. As expected, there is a first-order transition from a nearly parallel conformation to a radial conformation at a critical value of WR/K; the critical value of WR/K is about 5.95, which is somewhat larger than the value of 3 that follows from the simple analysis above based on a transition from a perfectly parallel alignment.

The equilibrium director orientation distribution is shown for $WR/K=4.2$ (nearly parallel) and $WR/K=6.0$ (radial) in

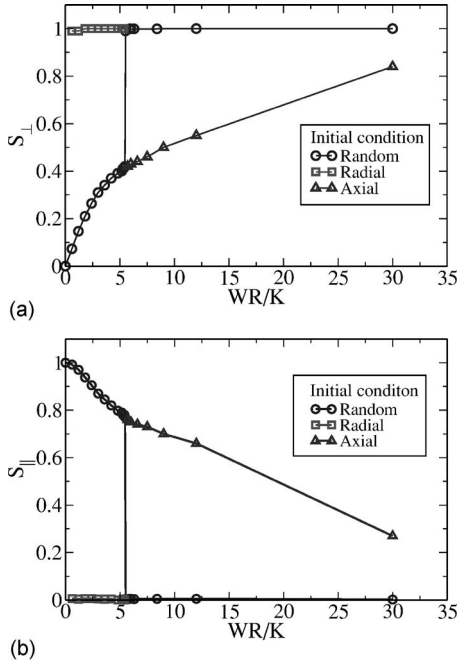

FIG. 4. (a) Radial ($S_{\perp}$) and (b) global ($S_{\|}$) order parameters for a spherical nematic drop with homeotropic anchoring and equal elastic coefficients as functions of WR/K. (○) Global minimum. (□) Radial local minimum. (△) Axial local minimum.

Figs. 2(a) and 2(b), respectively. These are planar cuts orthogonal to one axis, and the orientation distribution for $WR/K=4.2$ would have a different appearance on another

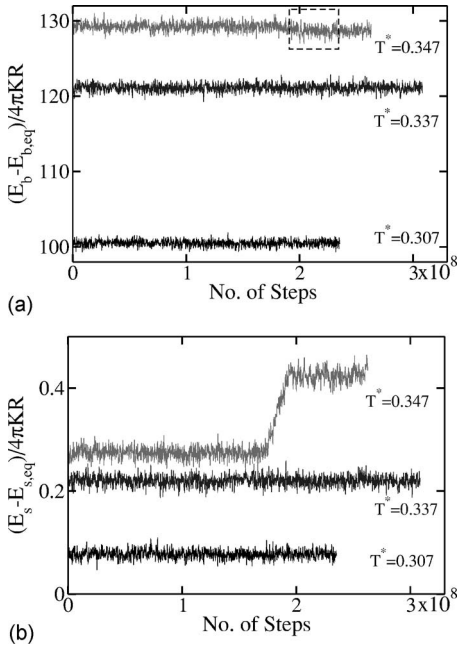

FIG. 5. Bulk and surface free energies for equal elastic coefficients with $WR/K=3.6$ at different values of reduced Monte Carlo temperature $T^*=k_BT/Kl$. Average bulk energies before and after the transformation are $\langle(E_b-E_{b,\mathrm{eq}})\rangle/4\pi KR=129.25$ and 128.65, respectively, while average surface energies before and after the transformation are $\langle(E_s-E_{s,\mathrm{eq}})\rangle/4\pi KR=0.27$ and 0.42, respectively.

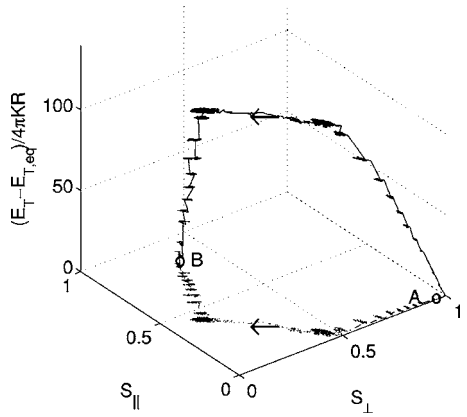

FIG. 6. Path in conformation space and corresponding energy in passing from a locally stable radial conformation (A) to the aligned free energy minimum state (B).

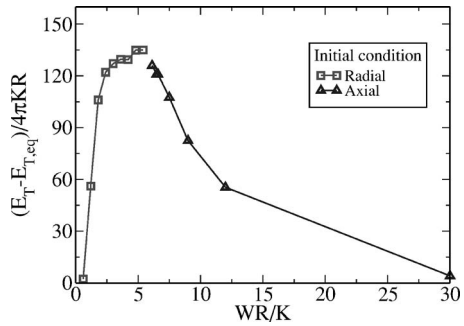

FIG. 7. Estimated energy barrier as a function of WR/K.

plane. Droplet order can be visualized more easily using simulated polarized optical micrographs. We use a standard matrix approach, similar to, for example, Berggren *et al.* [22], with a Jones matrix formalism [2,23]. The transmitted intensities shown here were calculated from the full three-dimensional distributions (shown in one plane in Fig. 2) by assuming that the light has a wavelength of 0.55 μm, and that the ordinary and extraordinary indices of refraction are 1.5 and 1.7, respectively. Simulated images for $WR/K=4.2$ and 6.0 are shown in Figs. 3(a) and 3(b), respectively. The radial morphology is clearly revealed through the classic Maltese cross image in Fig. 3(b). The details of the image for the parallel orientation will depend on the relative angle of the simulated polarized light beam and the mean orientation direction.

B. Multiplicity

We have found that other locally stable states may exist for equal elastic coefficients by starting simulated annealing calculations with a radial distribution when WR/K is less

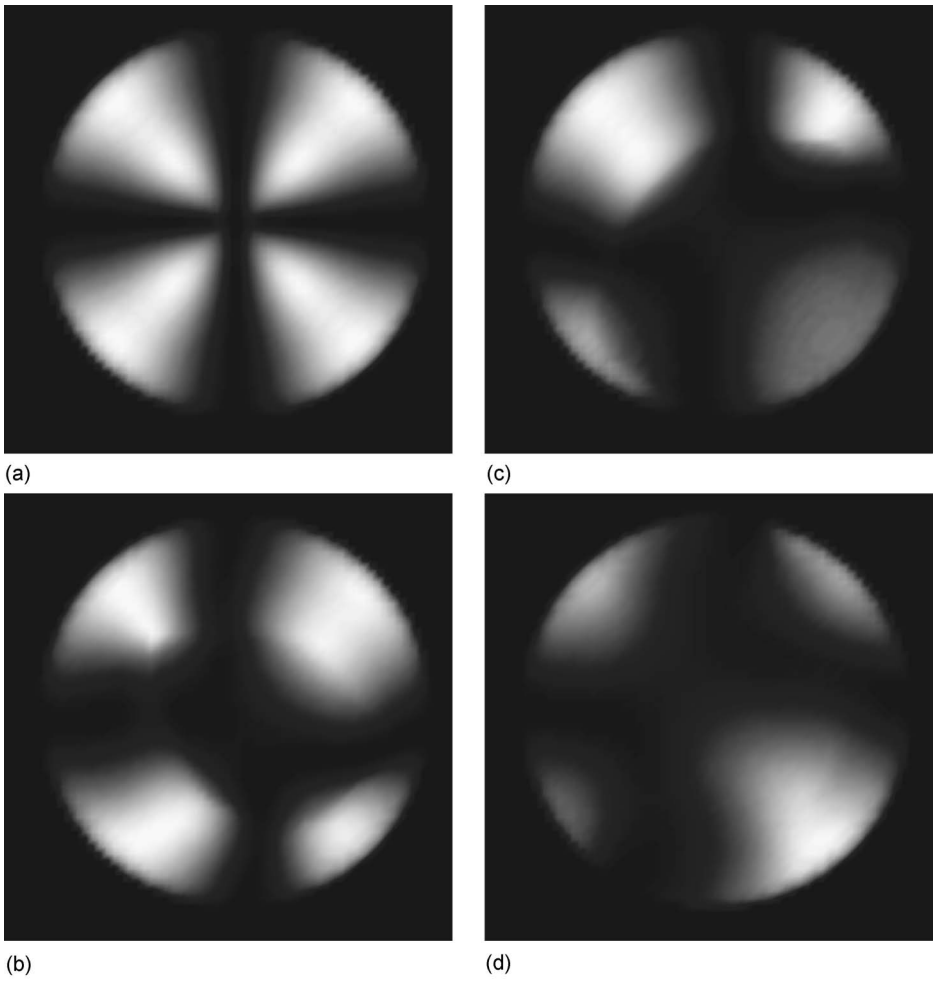

FIG. 8. (a)–(d) Defect development during the transition from a locally stable radial conformation to the equilibrium axial conformation; $WR/K=5.1$.

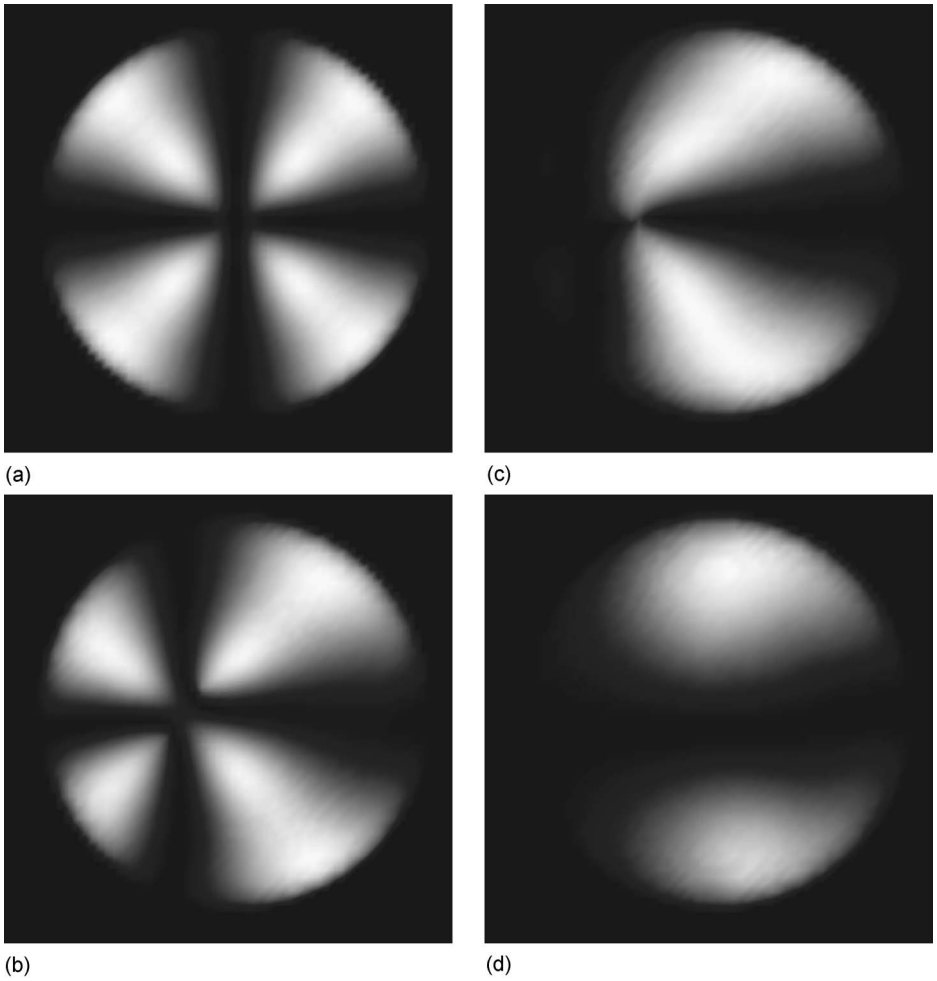

FIG. 9. (a)–(d) Defect development and transition between a locally stable radial conformation and an equilibrium axial conformation; $WR/K=0.6$. The final state, which is completely dark except for a thin region near the surface, is not shown.

than the transition value and with a near-axial distribution when WR/K is greater than the transition value, keeping the Monte Carlo temperature (hence the fluctuations) small. In such cases we obtain convergence to a second local minimum in free energy; in the former case the local free energy state is radial, while in the latter it is a parallel state with increasing distortion as WR/K is increased. The order parameters for both the global and local minima are shown in Fig. 4, using 82 696 lattice cells as a compromise between accuracy and computational efficiency.

The complementary order parameters $S_{\parallel}$ and $S_{\perp}$ comprise a minimal description of the droplet morphology. The simulations converge to a local free energy minimum at each value of the Monte Carlo temperature for a given WR/K and specified starting conditions, and each of these converged states is characterized by a unique pair $(S_{\parallel},S_{\perp})$. Hence incremental changes in the Monte Carlo temperature, starting from a local minimum, will provide a path through the conformation space along a sequence of feasible quasistatic states; this path can be tailored to lead to the global minimum by first increasing the Monte Carlo temperature until the morphology has changed from one qualitative type to the other, then decreasing the temperature to reach the equilibrium state. Figure 5, for example, shows the bulk and surface energies at $WR/K=3.6$ for a succession of successful Monte Carlo steps at increasing dimensionless Monte Carlo (MC) temperatures $T^*=k_BT/Kl$, where T is the MC temperature. The transition from a radial conformation to an orientation with substantial alignment occurs for T^* between 0.337 and 0.347. (A nematic-isotropic transition occurs at $T^*=0.375$.) The small increase in the surface energy $(0.6\pi KR)$ is offset by the small decrease $(2.4\pi KR)$ in the bulk energy, with a net change in the total free energy of only 0.35%. The sequence of states in the $S_{\parallel}$-$S_{\perp}$ plane, together with the corresponding free energies as a three-dimensional curve, are shown in Fig. 6. The transition between two states with similar energies, and the corresponding development of global alignment, is readily seen. The difference between the free energy of the initial state and the maximum free energy along the path is an upper bound for the height of the energy barrier between the local and global equilibrium states; it is only an upper bound because our algorithm gives a particular path through the conformation space, and another path might exist that has a lower barrier.

The estimated energy barrier is shown as a function of WR/K in Fig. 7. The maximum corresponds to an energy density of about 2000 J/m^3 (Pa) for a droplet with a radius of 1 μm and a typical elastic coefficient of 5×10^{-12} N. This energy density could be transmitted mechanically in a dilute suspension with a suspension viscosity of 50 Pa s at a shear rate of about 40 s^{-1}; it would require shear rates of the order of 80 000 s^{-1} for a suspension with a viscosity comparable to a typical nematic viscosity of 0.025 Pa s.

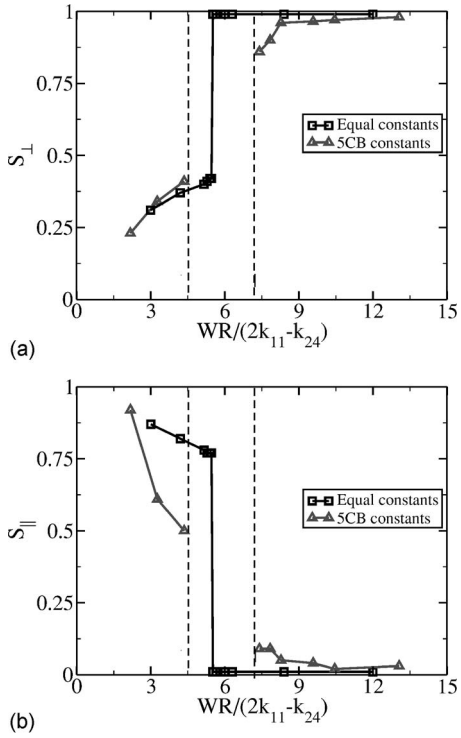

FIG. 10. (a) Radial order parameter $S_\perp$ and (b) global order parameter $S_\parallel$ as functions of anchoring strength parameter $WR/(2k_{11}-k_{24})$ for equal elastic coefficients and elastic coefficients characteristic of 5CB.

Figure 8 shows the progression of the structural change with Monte Carlo steps during the transition from a locally stable radial conformation to the stable aligned conformation at $WR/K=5.1$, which is close to the transition. Radial order is initially lost in the region of the singularity at the origin, and the parallel orientation then spreads outward to envelop the entire droplet. The sequence is different during a transition from radial to axial with weak anchoring, as shown in Fig. 9; in this case the singularity moves asymmetrically from the center towards a point on the surface as the parallel orientation develops. During a transition from an aligned conformation to a strong-anchoring global minimum (not shown), two defects originate at opposite poles and progress to the center.

C. Unequal elastic coefficients

We have examined the effect of the saddle-splay coefficient k_{24} by carrying out droplet calculations in which $k_{11}=k_{22}=k_{33}$ and the ratio k_{24}/k_{11} is varied between 2/3 and 4/3. The first-order transition between axial and radial conformations remains unchanged when WR/K is replaced by the parameter $WR/(2k_{11}-k_{24})$, although there are small differences in the axial order parameter prior to the transition.

The transition is broader, and the parallel and radial order before and after the transition less perfect because of the presence of twist distortions, when $k_{22}/k_{11}<1$. Figure 10 shows the order parameters $S_\parallel$ and $S_\perp$ as functions of $WR/(2k_{11}-k_{24})$ with $k_{33}/k_{11}=1.31$ and $k_{22}/k_{11}=0.51$ (typical of 5CB at room temperature) and $k_{24}=(k_{11}+k_{22})/2$, together with the curves for equal elastic coefficients. The minimum energy structures obtained in simulated annealing calculations starting from a random initial state in the region between the two dashed lines, roughly $4.5<WR/(2k_{11}-k_{24})<7.3$, were not consistently reproducible and often reflected "escaped" structures that differed significantly from the par-

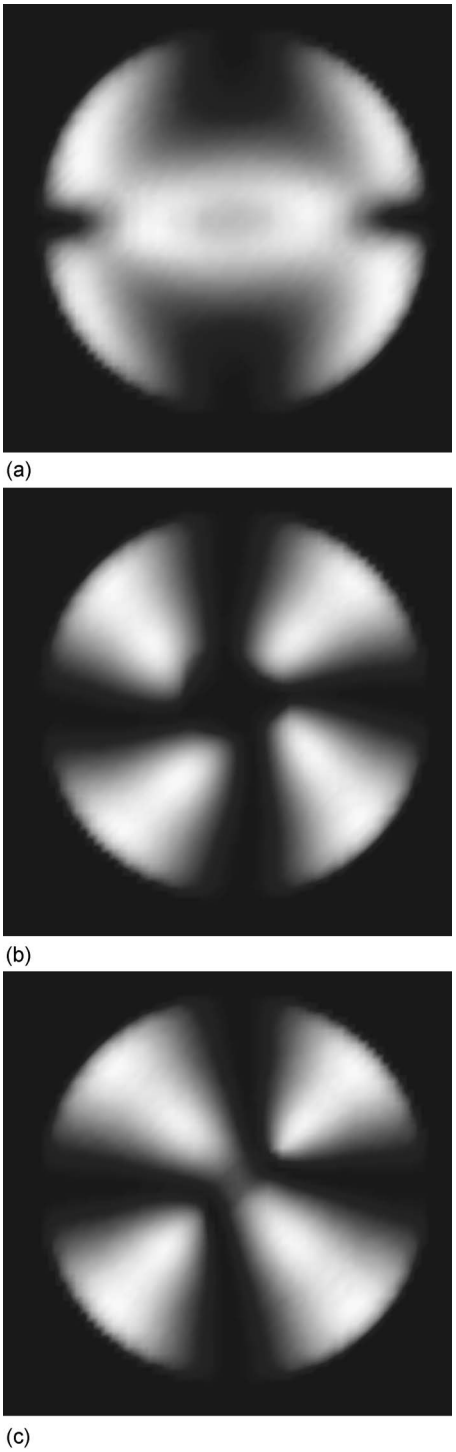

FIG. 11. Simulated optical micrographs for elastic constants characteristic of 5CB; $WR/(2k_{11}-k_{24})$ (a) 7.19, (b) 8.27, and (c) 21.77.

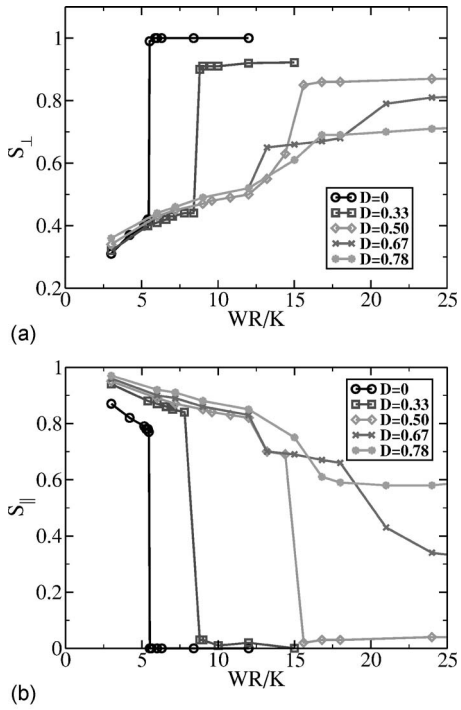

FIG. 12. (a) Orthogonal order parameter $S_\perp$ and (b) global order parameter $S_\parallel$ as functions of the anchoring strength parameter WR/K for spheroidal droplets at various values of the deformation parameter D.

allel or radial morphologies computed at lower and higher values of $WR/(2k_{11}-k_{24})$. The simulated micrograph in Fig. 11(a) shows one realization for $WR/(2k_{11}-k_{24})=7.19$, for example, in which there is a substantial core region with an escaped structure. Radial orientation is always achieved from a random initial condition at $WR/(2k_{11}-k_{24})=8.27$, but it is distorted by twist, as shown in Fig. 11(b). Some twist distortion persists even at extremely strong anchoring, as seen in Fig. 11(c) for $WR/(2k_{11}-k_{24})=21.8$, since the small ratio of twist to splay constants makes splay deformations energetically unfavorable.

IV. RESULTS FOR SPHEROIDAL DROPLETS

The order parameters for spheroidal droplets with equal elastic coefficients are shown in Figs. 12(a) and 12(b) as functions of WR/K for various values of $D=(L-B)/(L+B)$, where L and B are the major and minor axes of the spheroid, respectively. ($D=0.78$ corresponds to $L/B=8$, for example.) R is based on the radius of the sphere with the same volume. The transition is sharp for small values of D, but it becomes gradual for large extensions. This is because the orientation distribution in a highly elongated droplet with strong homeotropic anchoring is nearly parallel over a large fraction of the droplet volume. $S_\parallel$ and $S_\perp$ are nearly equal for $D=0.78$ with strong anchoring.

As with spherical droplets, the system can become trapped in a local minimum in the energy surface and exhibit multiplicity. Such trapping could occur physically by, say, deforming a sphere with homeotropic anchoring that has a

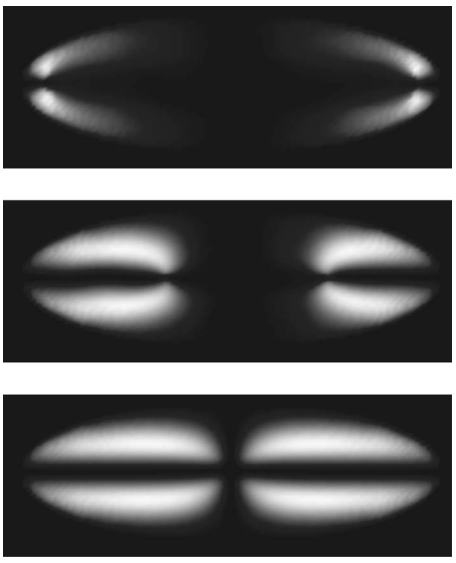

FIG. 13. (a)–(c) Transition from a parallel conformation to the equilibrium orthogonal conformation; $WR/K=30$; $D=0.5$.

radial orientation to a value of D such that a parallel orientation is the minimum energy state. (This would occur, for example, if a sphere with $WR/K=10$ were to be deformed to a spheroid with $D\geqslant 0.67$.) As with the spherical droplets, we have estimated the energy barrier between the local and global minima by initializing the system in the local minimum and then gradually increasing the Monte Carlo temperature until the transition occurs. Figure 13, for example, shows the structural evolution from a droplet with a parallel distribution [Fig. 13(a)] to the globally stable orthogonal distribution with a singularity at the center [Fig. 13(c)] for $WR/K=30$ and $D=0.5$. Figure 13(b) is an intermediate state that persists during the transition and seems to occupy a local minimum; here, two singularities separate orthogonal end regions from an essentially parallel center. The reverse process is observed for very strong anchoring, where the lowest energy state for a large elongation is parallel; in this case the center singularity from the radial spherical droplet separates into two singularities that migrate to the ends during the transition to the parallel orientation. The estimated energy barriers as functions of WR/K are shown in Fig. 14 for spheroids with D ranging from 0 to 0.78. The broken lines indicate small ranges of WR/K where the algorithm was not effective be-

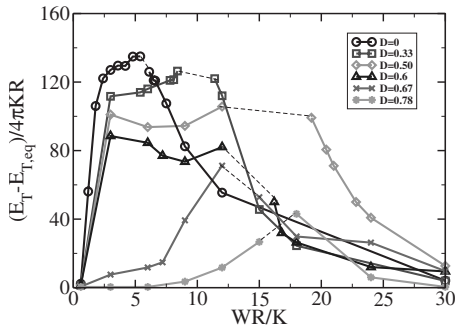

FIG. 14. Estimated energy barriers as functions of WR/K for spheroids with various values of D.

cause of the absence of a large shift in the values of the order parameter pairs. The maximum transition energy is substantially reduced by elongation to aspect ratios of four or more ($D \geqslant 0.6$).

V. CONCLUSIONS

Simulated annealing is an effective computational scheme for calculating minimum free energy orientation distributions and transitions between local mimina in the energy landscape of liquid crystalline droplets. The simulation results establish the morphological richness of these droplets, even in the approximation of equal elastic coefficients. Multiple steady states that are separated by finite energy barriers exist for spherical and spheroidal droplets with homeotropic anchoring over the entire range of the dimensionless ratio of surface to elastic forces, with maximum transition energy densities of the order of 2000 J/m^3 (Pa) for a typical liquid crystalline droplet with a spherical radius of 1 μm. The transition energy density decreases with elongation to aspect ratios of four or more, indicating that elongation is favored to drive surface-induced transitions.

ACKNOWLEDGMENTS

This work was supported by the National Science Foundation. Dr. Xianfeng Li provided valuable input during the early stages of the work, and we are grateful to Professor Mark Shattuck and Professor Oleg Lavrentovich for insightful discussions.

[1] O. D. Lavrentovich, Liq. Cryst. **24**, 117 (1998).
[2] P. S. Drzaic, *Liquid Crystal Dispersions* (World Scientific, Singapore, 1995).
[3] Y. W. Inn and M. M. Denn, J. Rheol. **49**, 887 (2005).
[4] M. Kleman and O. D. Lavrentovich, *Soft Matter Physics* (Springer, New York, 2003), Chap. 5.
[5] P. P. Karat and N. V. Madhusudana, Mol. Cryst. Liq. Cryst. **36**, 51 (1976).
[6] R. D. Polak, G. P. Crawford, B. C. Kostival, J. W. Doane, and S. Zumer, Phys. Rev. E **49**, R978 (1994).
[7] T. De'nève, M. Kleman, and P. Navard, Liq. Cryst. **18**, 67 (1995).
[8] G. P. Crawford and S. Žumer, Int. J. Mod. Phys. B **9**, 2469 (1995).
[9] J. L. Ericksen, Phys. Fluids **9**, 205 (1966).
[10] J. Nehring and A. Saupe, J. Chem. Phys. **54**, 337 (1971).
[11] A. Rapini and M. Papoular, J. Phys. (Paris), Colloq. **30**, C4 (1969).
[12] M. Heppenstall-Butler, A. W. Williamson, and E. M. Terentjev, Liq. Cryst. **32**, 77 (2005).
[13] T. Tixier, M. Heppenstall-Butler, and E. M. Terentjev, Langmuir **22**, 2365 (2006).
[14] P. A. Lebwohl and G. Lasher, Phys. Rev. A **6**, 426 (1972).
[15] C. Chiccoli, P. Pasini, F. Semeria, and C. Zannoni, Mol. Cryst. Liq. Cryst. Sci. Technol., Sect. A **212**, 197 (1992).
[16] J. Lu, H. Zhang, J. Ding, and Y. Yang, Sci. China, Ser. B: Chem. **39**, 203 (1996).
[17] N. V. Priezjev and R. A. Pelcovits, Phys. Rev. E **63**, 062702 (2001).
[18] J. Hobdell and A. Windle, Liq. Cryst. **23**, 157 (1997).
[19] T. Gruhn and S. Hess, Z. Naturforsch., A: Phys. Sci. **51a**, 1 (1996).
[20] C. Zannoni, in *The Molecular Physics of Liquid Crystals*, edited by G. R. Luckhurst and G. W. Gray (Academic Press, New York, 1979), p. 191.
[21] C. Chiccoli, P. Pasini, F. Semeria, and C. Zannoni, Phys. Lett. A **150**, 311 (1990).
[22] E. Berggren, C. Zannoni, C. Chiccoli, P. Pasini, and F. Semeria, Phys. Rev. E **50**, 2929 (1994).
[23] G. Fuller, *Optical Rheometry of Complex Fluids* (Oxford University Press, New York, 1995).